Research Article | Vol. 30, No. 2 / 17 Jan 2022 / Optics Express 2748
Optics EXPRESS

Specific features of the VCSEL spectra under microwave current modulation

E. A. Tsygankov,[1,*] S. A. Zibrov,[1] M. I. Vaskovskaya,[1] D. S. Chuchelov,[1] V. V. Vassiliev,[1] V. L. Velichansky,[1] A. E. Drakin,[1] and A. P. Bogatov[1]

[1]The Lebedev Physical Institute of the Russian Academy of Sciences, Moscow 119991, Russia
[*]selentinthebright@gmail.com

Abstract: The optical spectrum of a vertical-cavity surface-emitting laser under microwave frequency current modulation is asymmetric in most cases, i.e., sidebands equidistant from the carrier have unequal powers. Spectra asymmetry is conventionally explained as a result of amplitude modulation affecting a phase-modulated field, but this approach does not give a comprehensive description of the asymmetry. We performed a sequential analysis based on Maxwell's equations accounting for the nonlinear interaction of five spectral components of the laser field. This approach predicted a non-global asymmetry of the spectrum and a new resonant feature in the dependence of the second sidebands' power ratio on the injection current, which we demonstrate experimentally.

1. Introduction

The vertical-cavity surface-emitting laser (VCSEL) is one of the essential elements of a chip-scale atomic clock [1]. Microwave modulation of its injection current provides a polychromatic optical field for excitation of the metrological coherent population trapping (CPT) resonance. The modulation frequency is equal to half of the ground-state hyperfine splitting of alkali-metal atoms. The resonant (first-order) sidebands are tuned to the hyperfine components of the D_1 absorption line and pump an atomic ensemble into the dark state. One of the main characteristics of an atomic clock is frequency stability and among its limiting factors is frequency drift due to the light shift [2–6]. Since the carrier and the first sidebands of laser spectrum induce the light shift of the opposite sign than higher-order spectral components, suppression of the total shift is possible at a particular value of the deep modulation power (more than five spectral components) [7–13] (if a buffer gas pressure is not too high [14]). The clocks' frequency stability also depends on the CPT resonance contrast [5], which reaches a maximum when intensities of the resonant sidebands are equal (at their total fixed power) [1,15,16]. In practice, the lasers usually have asymmetric spectra with unequal powers of the first-order sidebands, which also leads to asymmetry of the CPT resonance. Our recent research found that in this case the resonance frequency acquires shift, which has a complex dependence on the light power [17]. Therefore for metrological calculations of the CPT resonance characteristics, we require an approach giving the correct distribution of the laser power between spectral components and their asymmetry.

There is a standard explanation that the asymmetry stem from an amplitude modulation (AM) accompanying the phase modulation (PhM) of a laser field [18–39]. Assuming this model, some researchers [28–30,33] evaluate PhM and AM indices and the relative phase shift between the modulations via the ratios of the first-order sidebands powers to the carrier power.

We investigate spectra of the field undergoing PhM and AM (section 2) and demonstrate that they have different asymmetry than current-modulated VCSELs (section 3). Further, in section 4, we present the theory based on Maxwell's equations and derive the solution for powers of the second sidebands under the small-signal approximation. We get that the ratio of their powers has

#445327 https://doi.org/10.1364/OE.445327
Journal © 2022 Received 8 Oct 2021; revised 1 Jan 2022; accepted 2 Jan 2022; published 12 Jan 2022

Optics EXPRESS

a resonant behavior as a function of the injection current and demonstrate it experimentally for lasers of different manufacturers.

2. Spectra of the PhM and AM field

We analyze the following field whose phase and amplitude are under modulation:

$$\mathcal{E}(t) = \mathcal{E}\left(1 + M\sin(\Omega t + \varphi)\right) \cdot \cos\left(\omega t + a\sin\Omega t\right). \tag{1}$$

Let us briefly outline the reasoning for the derivation of Eq. (1). The field amplitude is determined by the injection current of a diode laser, thus its modulation provides AM. The refractive index also oscillates at the modulation frequency since it depends on temperature and (at high frequencies) on the electron concentration, which gives PhM. Since the responses are not synchronous (due to relaxation processes, gain saturation, and other factors), the relative phase shift between modulations is accounted for by φ.

For analysis of Eq. (1) we take into account that the carrier frequency ω is much greater than the modulation frequency Ω, $\omega \gg \Omega$; and the parameter φ can take values within interval $[-\pi/2, \pi/2]$. The last parameter determines whether the field 1 spectrum is symmetric, i.e., whether the powers of sidebands $|k|$ and $-|k|$ ($k \neq 0$), oscillating at the frequencies $\omega \pm |k|\Omega$, are equal. We express the sideband k amplitude via a, M, φ using the well-known relation $\cos(\omega t + a\sin\Omega t) = \sum_k J_k(a)\cos(\omega + k\Omega)t$, where $J_k(a)$ is the Bessel function of the first kind. We consider the values of the modulation indices as arbitrary, i.e., we hold all Bessel functions in the Fourier expansion to account for all spectral components of field Eq. (1). Then employing the recurrent relations $J_{k-1}(a) + J_{k+1}(a) = 2kJ_k(a)/a$ and $J_{k-1}(a) - J_{k+1}(a) = 2\partial J_k(a)/\partial a$ we get the following function determining the sideband k power, P_k:

$$P_k \propto \mathcal{F}_k = J_k^2(a)\left(1 + \frac{kM\sin\varphi}{a}\right)^2 + \left(M\cos\varphi\frac{\partial J_k(a)}{\partial a}\right)^2. \tag{2}$$

The subject of our analysis is the possibility to describe the modulated VCSEL spectra via field Eq. (1). An unambiguous criterion is the correspondence of symmetries for field Eq. (1) spectra and those of current-modulated VCSEL. We define symmetry as the fulfillment of the condition $\mathcal{F}_{|k|}/\mathcal{F}_{-|k|} - 1 = 0$ for all k. If it does not hold for any k, then we call the spectrum asymmetric. As follows from formula (2), $\mathcal{F}_{|k|}/\mathcal{F}_{-|k|} - 1$ has either positive sign ($\sin\varphi > 0$), or negative ($\sin\varphi < 0$) for all k. We will refer to these cases as global asymmetry. For $\sin\varphi = \pm 1$ the spectrum is the most asymmetric (at fixed values of a and M, the value of $\mathcal{F}_{|k|}/\mathcal{F}_{-|k|} - 1$ is maximal or minimal, respectively), and the power of each sideband k turns to zero at $J_k(a) = 0$ as in the case of PhM ($M = 0$); see Fig. 1(a).

On the opposite, for $\sin\varphi = 0$ the spectrum is symmetric, see Fig. 1(b). In a close vicinity of $\varphi = 0$ the measure of asymmetry can be estimated as $\mathcal{F}_{|k|}/\mathcal{F}_{-|k|} - 1 \simeq 4|k|\varphi M/a$. The power of each sideband can not be equal to zero since the Bessel functions $J_k(a)$ and $J_k'(a)$ do not turn to zero simultaneously. The aforementioned asymmetry of the field Eq. (1) spectra has the following qualitative explanation. When the relative phase shift between both modulations is such that the amplitude and frequency of the field increase simultaneously, then the power of each sideband $|k|$ is greater than that of sideband $-|k|$. When the amplitude change is out of phase with the frequency change, the asymmetry of spectra is the opposite. We note that in some cases, for example, see [27], the term in the first brackets of Eq. (1) is taken as $\sqrt{1 + M\sin(\Omega t + \varphi)}$, but such a description of AM does not change the symmetry of the field with PhM and AM.

In the following section, we compare examples of the VCSEL spectra with those of field 1.

Optics EXPRESS

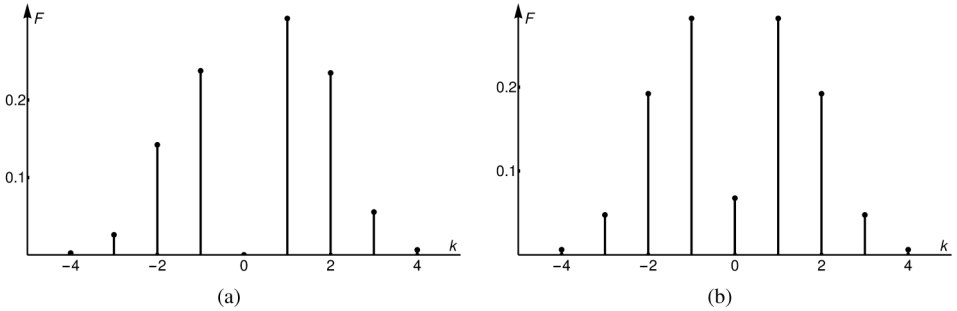

Fig. 1. Values of functions $\mathcal{F}_{-4}, \ldots, \mathcal{F}_4$ at (a) $a = 2.4$, $M = 0.15$, $\sin\varphi = 1$ and (b) $a = 2.4$, $M = 0.5$, $\sin\varphi = 0$. (a) The spectrum has the global asymmetry. The carrier amplitude is equal to zero as in the case of the single PhM ($M = 0$). (b) The spectrum is symmetric. The carrier amplitude is not equal to zero in spite of that $J_0(2.4) \simeq 0$ due to the second term on the right-hand side of Eq. (2).

Table 1. Typical optical and electric characteristics of the used VCSELs

Laser	Threshold current, mA	Recommended operating current, mA	Maximum output power, mW	Side mode suppression ratio, dB/Hz
ULM	0.5	2.0	0.25 . . . 1	>25
Princeton Optronics	0.3	5.0	3.0	35
Thorlabs	0.5	2.0	0.4	>20

3. Experiment

The experimental setup is shown in Fig. 2. We use 795 nm VCSELs from three different companies: Philips Photonics (ULM Photonics), Princeton Optronics, and Thorlabs. Typical values of the threshold current, operating current, output power and side mode suppression ratio of the used lasers are given in Table 1. All VCSELs are housed in a TO-46 package and operate at 20°C. The radiation passing through an optical isolator is divided by a beam splitter into two optical channels. The laser spectrum is registered by a photodetector PD1 and a 35 GHz scanning Fabry-Perot interferometer (FPI) consisting of two parallel flat mirrors with a reflectivity of 92%. The L/I curve is monitored by a photodetector PD2. The laser injection current is modulated by the Agilent 8257D frequency synthesizer at a frequency of 3 GHz. RF modulation and DC

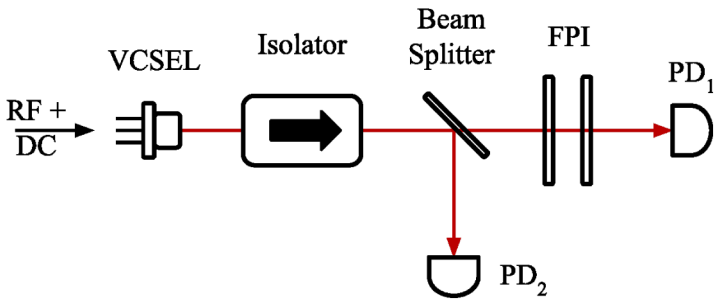

Fig. 2. The layout of the experimental setup. VCSEL is a vertical-cavity surface-emitting laser, FPI is Fabry-Perot interferometer, PD1,2 are photodetectors. The generator provides the RF signal for current modulation.

Optics EXPRESS

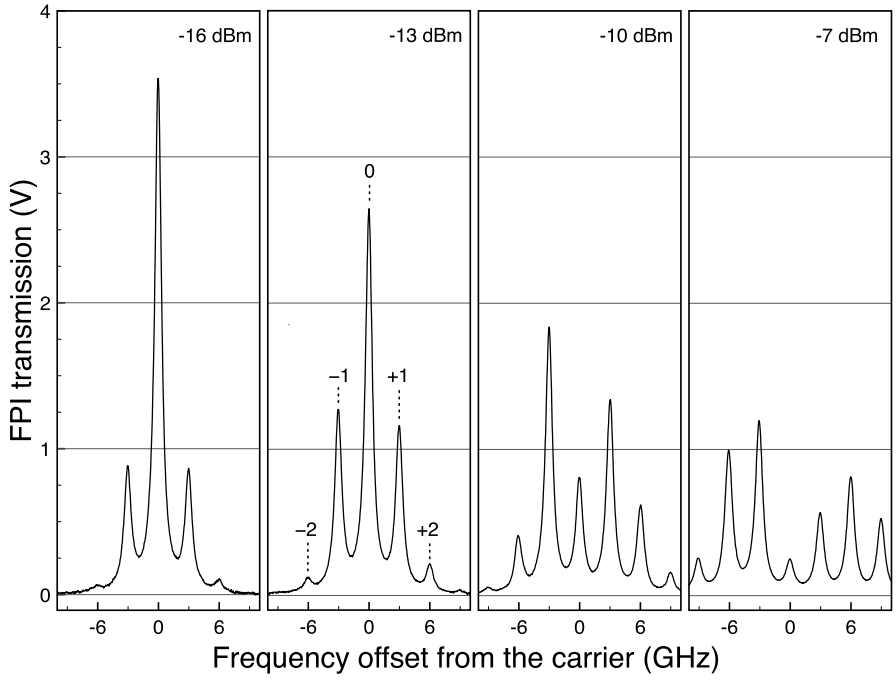

Fig. 3. Philips Photonics VCSEL spectra obtained for different RF powers. The sidebands indices are denoted as "$0, \pm 1, \pm 2$". The type of asymmetry is not global for all observed spectra.

injection current are combined and fed to the laser with the Minicircuits ZFBT-6GW-FT+ bias tee. The results presented below refer only to lasers that operate stably in a single-mode regime with suppression of an orthogonally polarized mode by more than 20 dB [40].

Typical modulation spectra of a Phillips Photonics laser for various RF powers are shown in Fig. 3. Here and below, we indicate RF power at the output of the synthesizer. The operation current is 1 mA (the threshold current is 0.6 mA), and the corresponding radiation power is 160 μW. One can see from Fig. 3 that no general rule describing the asymmetry of sidebands of the same order can be made. The powers of the first order sidebands (± 1) in Fig. 3 are almost equal at -16 dBm, but with an increase in the RF power, the power of the long-wavelength component becomes greater than of the short-wavelength one. At the same time, at -13 dBm and at -10 dBm, the power of the short-wavelength second-order sideband ($+2$) exceeds the amplitude of the long-wavelength sideband (-2). At even higher RF powers (more than -7 dBm), the asymmetry of the second order sidebands changes (long-wavelength becomes greater than short-wavelength). Such behavior of the sidebands cannot be described in terms of the PhM-AM model.

4. Approach based on Maxwell's equations

The approach involves solving a coupled system of equations for field $E(r,t)$ and the electron concentration in the active media. Namely, one should solve Maxwell's equations for field $\mathcal{E}(r,t)$ with the boundary conditions in the laser cavity and the balance equation for the electron concentration $N(r,t)$ with modulated injection current $J(t) = J + mJ(e^{-i\Omega t} + \text{c.c.})$, where Ω is the modulation frequency. Since the electron concentration and the dielectric permittivity become periodic functions of Ω, the field $E(r,t)$ will also contain terms oscillating at multiples of Ω. Authors of Ref. [41] have implemented this approach for low modulation depth of the injection

Optics EXPRESS

current, treating terms $\propto m$ as much less than unity, accounting only for the first sidebands. They found the analytical solution with equal powers. In this section, we make the minimal expansion of this small-signal approximation model on terms $\propto m^2$ attempting to find a specific type of asymmetry for spectra having lower powers of components $k = \mp 2$ than $k = 0$, $k = \mp 1$. We do it since the equations for deep current modulation that give many sidebands can be solved only numerically.

We consider the modulated injection current as $J(t) = J + mJ(e^{-i\Omega t} + \text{c.c.})$ and represent the electron concentration in the factorized form, $N(r,t) = N(t)f(r)$. Dimensionless parameter m characterizes the ratio of AC and DC amplitudes. Also, the shape of $f(r)$ is assumed to be the same for all allowable values of injection current and corresponding values of the output laser power. This approximation is suitable for VCSEL since the active-region dimensions do not exceed the electron diffusion length significantly.

As was noted above, field $E(r,t)$ becomes a periodic function of Ω due to the injection current modulation. Since we consider m as a small parameter but hold second-order terms over m, we seek a solution for $E(r,t)$ in the following form:

$$E(r,t) = \frac{1}{2}\left(\mathbf{u}(r)\sum_{k=-2}^{2}\mathcal{E}_k e^{-i(\omega_0+k\Omega)t} + c.c.\right), \tag{3}$$

where ω_0 is the carrier frequency and $\mathcal{E}_{\mp 2} \propto m^2$, $\mathcal{E}_{\mp 1} \propto m$ and complex vector-function $\mathbf{u}(r)$ characterizes the spatial distribution of the amplitude over the volume V. It is bounded by the laser exit surface S_{out} from the one side and surface S_{bound} on all other sides. We use the factorized form for field Eq. (3) due to the experimental fact that the spatial configuration of the laser radiation does not depend on the output laser power and also on the modulation depth under the suppression of transverse modes. In addition, we consider $\mathbf{u}(r)$ as known from a steady-state solution of Maxwell's equations for the independent problem with the monochromatic field, namely:

$$\nabla \times \nabla \times \mathbf{u}(r) = k_0^2 \varepsilon_0 \left[r, N_s(r), \omega_0\right]\mathbf{u}(r),$$

where $N_s(r)$ is the electron concentration in the steady-state regime.

Then, normalizing $u(r)$ in the active region center so that $|\mathbf{u}(0,\,0,\,0)|^2 = 1$, we can write the balance equation for the active region centre as:

$$\frac{dN(t)}{dt} + \frac{N(t)}{\tau} + \frac{\sigma c n\left[N(t) - N_{tr}\right]}{8\pi\hbar\omega}\left|\sum_{k=-2}^{2}\mathcal{E}_k e^{-i(\omega_0+k\Omega)t}\right|^2 = \frac{J(t)}{eV_{act}}, \tag{4}$$

where τ is the electron lifetime in the excited state; N_{tr} is the electron concentration at the transparency; V_{act} is the effective volume of the active region. One should integrate $V_{act} = \int_V f(r)dV$ over the volume V.

It is also necessary to consider the terms oscillating at the doubled modulation frequency in the electron concentration, which arises due to nonlinear interaction of the optical field components in the laser medium: $N(t) = N_{th} + (\delta N' e^{-i\Omega t} + \delta N'' e^{-2i\Omega t} + c.c.)$, where $\delta N' \propto m$, $\delta N'' \propto m^2$. Substituting the expressions for $E(r,t)$ and $N(t)$ in Eq. (4) and separating the terms oscillating at different frequencies, we obtain:

$$\frac{N_{th}}{\tau} + \tilde{\sigma}\left(N_{th} - N_{tr}\right)\sum_{k=-1}^{1}|\mathcal{E}_k|^2 + \tilde{\sigma}\left(\delta N'\left[\mathcal{E}_{-1}\mathcal{E}_0^* + \mathcal{E}_0\mathcal{E}_1^*\right) + c.c.\right] = \frac{J}{eV_{act}}, \tag{5a}$$

$$\left(\frac{1}{\tau} - i\Omega + \tilde{\sigma}|\mathcal{E}_0|^2\right)\delta N' = m\frac{J}{eV_{act}} - \tilde{\sigma}\left(N_{th} - N_{tr}\right)\sum_{k=0}^{1}\mathcal{E}_{k-1}^*\mathcal{E}_k, \tag{5b}$$

Optics EXPRESS

$$\left(\frac{1}{\tau} - 2i\Omega + \tilde{\sigma}|\mathcal{E}_0|^2\right)\delta N'' = -\tilde{\sigma}\delta N' \sum_{k=0}^{1} \mathcal{E}^*_{k-1}\mathcal{E}_k - \tilde{\sigma}\left(N_{th} - N_{tr}\right) \sum_{k=0}^{2} \mathcal{E}^*_{k-2}\mathcal{E}_k. \tag{5c}$$

where we have introduced notation $\tilde{\sigma} = \sigma cn/(8\pi\hbar\omega)$. We note that the right part of the equation for $\delta N'$ contains source $mJ/(eV_{act})$ and term $\propto \left(\mathcal{E}^*_{-1}\mathcal{E}_0 + \mathcal{E}^*_0\mathcal{E}_1\right)$ indicating that the carrier and first sidebands nonlinearly interact in the active media modifying the amplitude of the electrons oscillations at frequency Ω. Also, the nonlinear interaction induces oscillation of electrons at frequency 2Ω.

Also, to write the equations for amplitudes of Eq. (3) we represent the dielectric permittivity in the following form

$$\varepsilon[r, t, N(r,t)] = \varepsilon_0[r, \omega_0, N_s(r)] + \left.\frac{\partial\varepsilon}{\partial\omega}\right|_{\omega=\omega_0} \Delta\omega + \left.\frac{\partial\varepsilon}{\partial N}\right|_{N=N_s(r)} \Delta N(r,t), \tag{6a}$$

$$\left.\frac{\partial\varepsilon}{\partial N}\right|_{N=N_s(r)} = -\frac{\sigma(\omega_0)n}{k_0}(R+i), \tag{6b}$$

where ω_0 and ε_0 are the frequency and permittivity in the single-mode regime; R is the non-dimensional phase-amplitude coupling factor; $\Delta N(r,t) = [N(t) - N_{th}]f(r)$. Using the expressions for $\varepsilon[r,t,N(r,t)]$ and $E(r,t)$ and making the same transformations as in Ref. [41], we get from Maxwell's equations:

$$-4\mathcal{E}_{-2}\frac{\Omega}{c}(1+\xi) + \mathcal{E}_{-1}k_0\Gamma\frac{\partial\varepsilon}{\partial N}(\delta N')^* + \mathcal{E}_0 k_0\Gamma\frac{\partial\varepsilon}{\partial N}(\delta N)^* = 0, \tag{7a}$$

$$-2\mathcal{E}_{-1}\frac{\Omega}{c}(1+\xi) + \mathcal{E}_0 k_0\Gamma\frac{\partial\varepsilon}{\partial N}(\delta N')^* = 0, \tag{7b}$$

$$2\mathcal{E}_1\frac{\Omega}{c}(1+\xi) + \mathcal{E}_0 k_0\Gamma\frac{\partial\varepsilon}{\partial N}\delta N' = 0, \tag{7c}$$

$$4\mathcal{E}_2\frac{\Omega}{c}(1+\xi) + \mathcal{E}_1 k_0\Gamma\frac{\partial\varepsilon}{\partial N}\delta N' + \mathcal{E}_0 k_0\Gamma\frac{\partial\varepsilon}{\partial N}\delta N'' = 0, \tag{7d}$$

where we have introduced coefficients $\xi = (\omega_0/2V_0)\int_V \mathbf{u}^2(r)\left.\frac{\partial\varepsilon}{\partial\omega}\right|_{\omega=\omega_0} dV$,

$\Gamma = (1/2V_0)\int_V |\mathbf{u}(r)|^2 f(r) dV$, $V_0 = \int_V \varepsilon_0|\mathbf{u}(r)|^2 dV$. Parameter ξ characterizes the contribution of the dispersion to the energy and its dissipation in the laser cavity, and Γ is the optical confinement factor [41]. Let us note that sources of sidebands amplitudes have contributions from the field scattering on oscillations of the electron concentration. For example, Stokes and anti-Stokes scattering of the carrier on electron oscillations at frequency 2Ω contributes to amplitudes of components $k = \mp 2$. These contributions compete with ones from scattering of the first sidebands on oscillations of the electron concentration at frequency Ω. There can be their non-equivalent constructive or destructive interference leading to a difference in amplitudes $\mathcal{E}_{-2}$ and $\mathcal{E}_2$. Since the field components scatter on oscillations of electrons and interact in the laser medium modifying amplitudes of oscillations, we can get the outcome of this interplay only by solving the coupled system of equations for the field and the medium.

To find the carrier amplitude, we put $\mathcal{E}^*_0 = \mathcal{E}_0$, which can always be achieved by introducing a phase shift into Eq. (3) and using replacement $\mathcal{E}_0^2 = \mathcal{A}_0^2 + m^2\mathcal{A}_2^2$. Then from Eq. (5a) we obtain two equations for the terms of the order of 1 and m^2:

$$\frac{N_{th}}{\tau} + \tilde{\sigma}(N_{th} - N_{tr})\mathcal{A}_0^2 = \frac{J}{eV_{act}}, \tag{8a}$$

$$(N_{th} - N_{tr})(|\mathcal{E}_{-1}|^2 + m^2\mathcal{A}_2^2 + |\mathcal{E}_1|^2) + \mathcal{A}_0\left[\delta N'(\mathcal{E}_{-1} + \mathcal{E}_1^*) + c.c.\right] = 0. \tag{8b}$$

Now $\mathcal{A}_0$ can be considered as a known value determined by the constant part of the injection current. We can also find the term $m^2\mathcal{A}_2^2$, which turns out to be negative, demonstrating that

Optics EXPRESS

the carrier power falls with an increase in the modulation depth. The other amplitudes can be expressed as $\mathcal{E}_{\mp2,\mp1} = \nu_{\mp2,\mp1}\mathcal{A}_0$ to write Eqs. (5b)–(5c) for $\delta N'$ and $\delta N''$ as (neglecting the higher-order terms compared to those $\propto m^2$):

$$\delta N' = \frac{M - (N_{th} - N_{tr})\tilde{\sigma}\mathcal{A}_0^2(\nu_{-1}^* + \nu_1)}{1/\tilde{\tau} - i\Omega}, \tag{9a}$$

$$\delta N = -\tilde{\sigma}\mathcal{A}_0^2\frac{\delta N'(\nu_{-1}^* + \nu_1) + (N_{th} - N_{tr})(\nu_{-2}^* + \nu_{-1}^*\nu_1 + \nu_2)}{1/\tilde{\tau} - 2i\Omega}, \tag{9b}$$

where $M = mJ/(eV_{act})$, $1/\tilde{\tau} = 1/\tau + \tilde{\sigma}\mathcal{A}_0^2$. Equations (9) and (7) allow us to find $\nu_{\mp1}, \nu_{\mp2}$. We get that powers of the first sidebands are equal, but for the second sidebands, we have:

$$\frac{\nu_2}{\nu_{-2}^*} = \frac{(R+i)\left\{\tilde{\tau}\tilde{\sigma}\mathcal{A}_0^2\left[\mathrm{Im}(\xi) - \mathrm{Re}(\xi) - 1\right]\left[\Omega_0(R-i) - 4\Omega(1-\xi^*)\right] + 2\Omega(i + 2\tilde{\tau}\Omega)(R+i)\,(1+\xi^*)^2\right\}}{(R-i)\left\{\tilde{\tau}\tilde{\sigma}\mathcal{A}_0^2\left[\mathrm{Im}(\xi) - \mathrm{Re}(\xi) - 1\right]\left[\Omega_0(R+i) + 4\Omega(1+\xi)\right] + 2\Omega(i + 2\tilde{\tau}\Omega)(R-i)\,(1+\xi)^2\right\}}, \tag{10}$$

where we introduced parameter $\Omega_0 = \sigma cn\Gamma(N_{th} - N_{tr})$, which depends on the relaxation oscillation frequency. Powers of the second sidebands are equal when the numerator and denominator in the formula above are complex conjugate values. It corresponds to the case $\tilde{\tau}\tilde{\sigma}\mathcal{A}_0^2 \ll 1$ where the spontaneous mechanism primarily determines the electron relaxation rate. If the stimulated one is large enough, then $\tilde{\tau}\tilde{\sigma}\mathcal{A}_0^2 \sim 1$, $|\nu_{-2}|^2 \neq |\nu_2|^2$ and the laser spectrum has special type of asymmetry: $|\nu_{-1}|^2 = |\nu_1|^2$, $|\nu_{-2}|^2 \neq |\nu_2|^2$. We remind that field Eq. (1) can have only the global asymmetry implying fulfillment of $|\nu_{-|k|}|^2 \neq |\nu_{|k|}|^2$ for all $k \neq 0$.

We neglect further the term ξ (whose absolute values of real and imaginary parts are smaller than 1) to simplify analytical expressions. In the case of small stimulated relaxation, $\tilde{\sigma}\mathcal{A}_0^2 \ll 1/\tau$, we get:

$$\frac{|\nu_2|^2}{|\nu_{-2}|^2} = 1 + \frac{4R}{1+R^2}\frac{4\tau\Omega + 1/\tilde{\Omega}}{1 + (2\tau\Omega)^2}\tau\tilde{\sigma}\mathcal{A}_0^2, \tag{11}$$

where $\tilde{\Omega} = \Omega/\Omega_0$. Thus, the power of the short-wavelength component is greater and the ratio grows with increase in injection current. To investigate the opposite case, we introduce parameter a_0 as $\tilde{\tau}\tilde{\sigma}\mathcal{A}_0^2 = 1 - a_0^2$. It tends to zero from above with growth of the stimulated relaxation for $\tilde{\sigma}\mathcal{A}_0^2 \gg 1/\tau$. Then, using linearization over a_0^2 and $\tilde{\tau}\Omega$, we get the same result:

$$\frac{|\nu_2|^2}{|\nu_{-2}|^2} = 1 + 16\frac{R\tilde{\Omega}(a_0^2 + 4\tilde{\Omega}\tilde{\tau}\Omega)}{(1+R^2)(1+4\tilde{\Omega}^2)}, \tag{12}$$

i.e., that the power of the short-wavelength component is greater. As follows from Eq. (12), the ratio tends to 1 from above with the injection current growth, indicating an extremum in dependence $|\nu_2/\nu_{-2}|^2$ on $\tilde{\sigma}\mathcal{A}_0^2$; see Fig. 4. By differentiating Eq. (10) over $\tilde{\sigma}\mathcal{A}_0^2$ and linearizing it over $\tilde{\Omega}$ we find the condition on maximum:

$$(2\Omega)^2 = \tilde{\sigma}\mathcal{A}_0^2\Omega_0 \equiv \frac{J - J_{th}}{eV_{act}}\sigma cn\Gamma, \tag{13}$$

where on the right-hand side of the equation we have the square of the relaxation oscillation frequency [42]. The maximum occurs when the doubled modulation frequency is close to it. We note that components of the optical field can acquire different phases due to the strong phase-amplitude coupling. Spectra become symmetric under neglecting of the latter; see Eqs. (11),(12), ratio $|\nu_2|^2/|\nu_{-2}|^2$ is equal to the unity for $R = 0$. As we indicated above, there can be the difference between powers of the second sidebands since they have two contributions from the scattering and phases of the first sidebands depend on $\tilde{\sigma}\mathcal{A}_0^2$ [41]. It turns out that the

Optics EXPRESS

contributions interfere more constructively for the short-wavelength sideband and this effect is the most prominent under fulfillment of condition (13). We remind that there is similar condition for the modulation efficiency, i.e., condition on where ratio $P_{\mp 1}/P_0$ is maximal as a function of the injection current at fixed RF power. Approach based on Maxwell's equations also describes this feature [41].

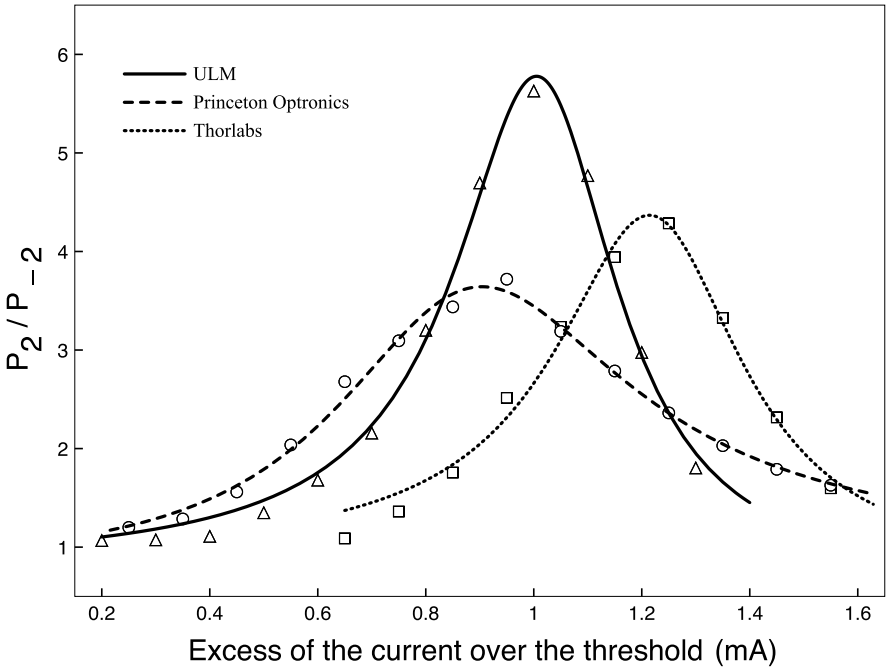

Fig. 4. Ratio of the second-order sidebands powers as a function of the injection current excess over the threshold. The threshold current is 0.6, 0.35, and 0.45 mA for lasers manufactured by ULM, Princeton Optronics, and Thorlabs. We used formula (10) to plot the theoretical curves.

An estimation of the radiation power P^* (inside the resonator) at which the stimulated and spontaneous decay rates are equal can be made via the photon flux density Φ since the relation $1/T^* = 1/\tau + \sigma\Phi$ holds for the electron lifetime T^*. Accounting for that $\Phi = P^*/(\hbar\omega S)$, where S is the laser beam square, we get formula $P^* = \hbar\omega S/(\tau\sigma)$. Taking for the estimation the wavelength of 795 nm, radius of the beam equal to 2 μm ($S = 4\pi \times 10^{-8}$ cm^2), $\tau = 10^{-9}$ s we obtain P^* of the order 300-60 mW for cross-section σ ranging from 1×10^{-16} to 5×10^{-16} cm^2. VCSEL output power can be more than 1000 times smaller than that in the cavity due to the large reflectivity of mirrors exceeding 0.995. Thus, there can be a difference in powers of the second sidebands at the total output radiation power of several tens of μW.

We check the prediction about the behavior of the second sidebands' powers experimentally. We tuned RF power for each value of the injection current to hold powers of the first components close to $P_0/4$. Under this condition, the lasers spectra had small but visible second sidebands (see Fig. 3 at −16 dBm). Figure 4 demonstrates dependence of ratio P_2/P_{-2} on the injection current for three lasers. We use parameters R, $\tau\Omega$, $\tilde{\Omega}$, $\mathcal{K}$, ξ to fit experimental data to the theory. Ratio $\tau\tilde{\sigma}\mathcal{A}_0^2$ was represented as $\mathcal{K}(J - J_{th})$. Thus, parameter $\mathcal{K}$ characterizes how quickly the rate of stimulated relaxation compared to spontaneous one grows as a function of the injection current. Values of the fitting parameters given in Table 2 are reasonable. For example, the electron lifetime is close to 1 ns for all lasers, which is consistent with the literature. Therefore,

Optics EXPRESS

the approach based on Maxwell's equations correctly describes the change in the powers ratio of small second components with an increase in the injection current.

Table 2. Values of the parameters used for fitting.

Laser	R	$\tau\Omega$, rad	$\tilde{\Omega}$	$\mathcal{K}$, mA^{-1}	ξ
ULM	6.25	15.44	$1.4 \cdot 10^{-1}$	6.86	$-0.2 + 0.08i$
Princeton Optronics	4.57	20.58	$2 \cdot 10^{-1}$	19.7	$0.14 + 0.15i$
Thorlabs	5.26	20.98	$9 \cdot 10^{-2}$	6.99	$0.15i$

Thus, the experimental spectra and sequential analysis based on Maxwell's equations demonstrate different type of asymmetry than the field undergoing PhM and AM. Additionally, we have found the resonant behaviour of ratio P_2/P_{-2} as the function of the injection current and observed it experimentally.

We note that the following treatment was made by Vahala and Yariv in works [43,44] to calculate the laser linewidth and the power fluctuations spectrum. At first, the authors of [43] took the dependence of the refractive index on the field intensity in algebraic form, as in the quasi-static models leading to optical field (1). Then, in [44], they took the dependence via differential equations, and the corresponding solution gave the physically adequate spectrum containing sidebands missing in [43]. They appear due to the scattering of laser radiation by dynamic fluctuations of the electron concentration. The presented theory similarly demonstrates that the VCSEL spectra have the feature missing in the models leading to a combination of the modulations.

5. Conclusion

There is a common explanation that asymmetry of VCSEL spectra stems from the admixture of an amplitude modulation to the phase one. We have analyzed the spectral symmetry of the optical field undergoing the simultaneous phase and amplitude modulations. It depends on the relative phase shift between these modulations: spectra can be symmetric or have the global asymmetry implying that the power of each $|k|$ sideband is greater or smaller than the power of corresponding $-|k|$ sideband, $k \neq 0$. We have shown that the VCSEL spectra have non-global asymmetry under the deep current modulation. They have a few pairs of sidebands equidistant from the carrier with a higher power of the short-wavelength component. And this inequality does not hold for other pairs of sidebands. Therefore we conclude that using the phase-amplitude modulated field for calculations of the CPT resonance parameters will give their distorted values since we require a deep current modulation to achieve the zero light shift. Considering atomic clocks, the error in the resonance frequency will be especially critical since it depends on the light shift and spectra asymmetry.

The presented theory based on Maxwell's equations explains asymmetry of VCSEL spectra as a result of scattering of the optical field components on oscillations of the electron concentration and their nonlinear interaction in the laser medium. When spectral component with frequency $\omega_0 + k\Omega$ scatters on electron oscillations at $n\Omega$ frequency, it makes contributions to amplitudes of components $k \mp n$ via Stokes and anti-Stokes mechanisms. Nonlinear interaction of spectral components induces oscillations of the electron concentration at multiples of Ω frequency. The theory considers coupled equations for the optical field and the medium providing the self-consistent approach. The solution under small-signal approximation gives spectra with non-global asymmetry and describes a resonant behavior for the ratio of the second sidebands powers as a function of the injection current. The ratio reaches maximum when doubled modulation and the relaxation oscillation frequencies are close to each other. We experimentally observe this specific feature for several lasers of different manufacturers.

Optics EXPRESS

We believe that the approach based on Maxwell's equations generalized for deep current modulation will allow us to model VCSEL spectra since it correctly describes some of their specific features already in the small-signal approximation. Also, we will investigate possibilities for manipulation of lasers spectra to obtain more high-quality CPT resonances.

Funding. Russian Science Foundation (19-12-00417).

Disclosures. The authors declare no conflicts of interest.

Data availability. Data underlying the results presented in this paper are not publicly available at this time but may be obtained from the authors upon reasonable request.

References

1. J. Kitching, "Chip-scale atomic devices," Appl. Phys. Rev. **5**(3), 031302 (2018).
2. S. Knappe, R. Wynands, J. Kitching, H. G. Robinson, and L. Hollberg, "Characterization of coherent population-trapping resonances as atomic frequency references," J. Opt. Soc. Am. B **18**(11), 1545–1553 (2001).
3. J. Vanier, "Atomic clocks based on coherent population trapping: a review," Appl. Phys. B **81**(4), 421–442 (2005).
4. V. Gerginov, S. Knappe, V. Shah, P. D. D. Schwindt, L. Hollberg, and J. Kitching, "Long-term frequency instability of atomic frequency references based on coherent population trapping and microfabricated vapor cells," J. Opt. Soc. Am. B **23**(4), 593–597 (2006).
5. V. Shah and J. Kitching, "Advances in coherent population trapping for atomic clocks," in *Advances in atomic, molecular, and optical physics*, E. Arimondo, P. Berman, and C. Lin, eds. (Academic Press, 2010), vol. 59, chap. 2, pp. 21–74.
6. A. Godone, F. Levi, C. E. Calosso, and S. Micalizio, "High-performing vapor-cell frequency standards," Nuovo Cimento Rivista Serie **38**, 133–171 (2015).
7. F. Levi, A. Godone, and J. Vanier, "The light shift effect in the coherent population trapping cesium maser," IEEE Trans. Ultrason., Ferroelect., Freq. Contr. **47**(2), 466–470 (2000).
8. M. Zhu and L. S. Cutler, "Theoretical and experimental study of light shift in a CPT-based Rb vapor cell frequency standard," in *Proceedings of 32nd Annual Precise Time and Time Interval (PTTI) Meeting*, Lee A. Breakiron, ed. (United States Naval Observatory, 2001), pp. 311–324.
9. V. Shah, V. Gerginov, P. D. D. Schwindt, S. Knappe, L. Hollberg, and J. Kitching, "Continuous light-shift correction in modulated coherent population trapping clocks," Appl. Phys. Lett. **89**(15), 151124 (2006).
10. E. E. Mikhailov, T. Horrom, N. Belcher, and I. Novikova, "Performance of a prototype atomic clock based on lin. ‖ lin. coherent population trapping resonances in Rb atomic vapor," J. Opt. Soc. Am. B **27**(3), 417–422 (2010).
11. R. Boudot, P. Dziuban, M. Hasegawa, R. K. Chutani, S. Galliou, V. Giordano, and C. Gorecki, "Coherent population trapping resonances in Cs–Ne vapor microcells for miniature clocks applications," J. Appl. Phys. **109**(1), 014912 (2011).
12. D. Miletic, C. Affolderbach, M. Hasegawa, R. Boudot, C. Gorecki, and G. Mileti, "AC Stark-shift in CPT-based Cs miniature atomic clocks," Appl. Phys. B **109**(1), 89–97 (2012).
13. D. S. Chuchelov, V. V. Vassiliev, M. I. Vaskovskaya, V. L. Velichansky, E. A. Tsygankov, S. A. Zibrov, S. V. Petropavlovsky, and V. P. Yakovlev, "Modulation spectroscopy of coherent population trapping resonance and light shifts," Phys. Scr. **93**(11), 114002 (2018).
14. M. I. Vaskovskaya, E. A. Tsygankov, D. S. Chuchelov, S. A. Zibrov, V. V. Vassiliev, and V. L. Velichansky, "Effect of the buffer gases on the light shift suppression possibility," Opt. Express **27**(24), 35856–35864 (2019).
15. M. Stähler, R. Wynands, S. Knappe, J. Kitching, L. Hollberg, A. Taichenachev, and V. Yudin, "Coherent population trapping resonances in thermal 85Rb vapor: D1 versus D2 line excitation," Opt. Lett. **27**(16), 1472–1474 (2002).
16. Z. Wang, K. Deng, D. He, X. Liu, L. Liu, T. Guo, and X. Chen, "Effects of the intensity difference of two laser fields on coherent population trapping clocks," in *2008 IEEE International Frequency Control Symposium*, (2008), 669–671.
17. D. S. Chuchelov, E. A. Tsygankov, M. I. Vaskovskaya, S. A. Zibrov, V. L. Velichansky, S. V. Petropavlovsky, and V. P. Yakovlev, "Study of factors affecting the light shift of the CPT resonance," J. Phys.: Conf. Ser. **1686**(1), 012029 (2020).
18. H. Olesen and G. Jacobsen, "A theoretical and experimental analysis of modulated laser fields and power spectra," IEEE J. Quantum Electron. **18**(12), 2069–2080 (1982).
19. S. Kobayashi, Y. Yamamoto, M. Ito, and T. Kimura, "Direct Frequency Modulation In AlGaAs Semiconductor Lasers," IEEE Trans. Microwave Theory Tech. **30**(4), 428–441 (1982).
20. W. Lenth, "High frequency heterodyne spectroscopy with current-modulated diode lasers," IEEE J. Quantum Electron. **20**(9), 1045–1050 (1984).
21. M. Gehrtz, G. C. Bjorklund, and E. A. Whittaker, "Quantum-limited laser frequency-modulation spectroscopy," J. Opt. Soc. Am. B **2**(9), 1510–1526 (1985).
22. X. Zhu and D. T. Cassidy, "Modulation spectroscopy with a semiconductor diode laser by injection-current modulation," J. Opt. Soc. Am. B **14**(8), 1945–1950 (1997).
23. R. Wynands and A. Nagel, "Inversion of frequency-modulation spectroscopy line shapes," J. Opt. Soc. Am. B **16**(10), 1617–1622 (1999).

Optics EXPRESS

24. A. Godone, F. Levi, S. Micalizio, and J. Vanier, "Dark-line in optically-thick vapors: Inversion phenomena and line width narrowing," Eur. Phys. J. D **18**(1), 5–13 (2002).
25. I. Ben-Aroya and G. Eisenstein, "Characterizing absorption spectrum of natural rubidium by using a directly modulated VCSEL," in *Proceedings of the 2005 IEEE International Frequency Control Symposium and Exposition*, 2005. (IEEE, 2005), pp. 602–607.
26. N. H. Zhu, T. Zhang, Y. L. Zhang, G. Zhi Xu, J. M. Wen, H. Pei Huang, Y. Liu, and L. Xie, "Estimation of frequency response of directly modulated lasers from optical spectra," J. Phys. D: Appl. Phys. **39**(21), 4578–4581 (2006).
27. C. M. Long and K. D. Choquette, "Optical characterization of a vertical cavity surface emitting laser for a coherent population trapping frequency reference," J. Appl. Phys. **103**(3), 033101 (2008).
28. A. Waxman, M. Givon, G. Aviv, D. Groswasser, and R. Folman, "Modulation enhancement of a laser diode in an external cavity," Appl. Phys. B: Lasers Opt. **95**(2), 301–305 (2009).
29. F. Gruet, A. Al-Samaneh, E. Kroemer, L. Bimboes, D. Miletic, C. Affolderbach, D. Wahl, R. Boudot, G. Mileti, and R. Michalzik, "Metrological characterization of custom-designed 894.6 nm VCSELs for miniature atomic clocks," Opt. Express **21**(5), 5781–5792 (2013).
30. A. Al-Samaneh, *VCSELs for Cesium-Based Miniaturized Atomic Clocks* (Books on Demand, 2015).
31. A. Stern, B. Levy, C. Levy, U. Arad, Y. Barash, R. Mann, and A. Gorelik, "The NAC-a miniature CPT Rubidium clock," in *2016 European Frequency and Time Forum (EFTF)*, (IEEE, 2016), pp. 1–4.
32. Y. Zhang, W. Yang, S. Zhang, and J. Zhao, "Rubidium chip-scale atomic clock with improved long-term stability through light intensity optimization and compensation for laser frequency detuning," J. Opt. Soc. Am. B **33**(8), 1756–1763 (2016).
33. J. A. Altabas, D. Izquierdo, J. A. Lazaro, and I. Garces, "Chirp-based direct phase modulation of VCSELs for cost-effective transceivers," Opt. Lett. **42**(3), 583–586 (2017).
34. M. Chakraborty and T. Chattopadhyay, "Optical Modulation Enhancement Through CW Injection Locking of a Sinusoidally Modulated Fabry-Perot Laser Diode," J. Opt. Commun. **39**(4), 393–400 (2018).
35. A. O. Makarov, S. M. Ignatovich, V. I. Vishnyakov, I. S. Mesenzova, D. V. Brazhnikov, N. L. Kvashnin, and M. N. Skvortsov, "Investigation of commercial 894.6 nm vertical-cavity surface-emitting lasers for applications in quantum metrology," AIP Conf. Proc. **2098**, 020010 (2019).
36. Z. Warren, H. Kettering, P. Ionov, A. Stapleton, and J. Camparo, "A versatile testbed for CubeSat atomic clock development: EOM vs Laser current modulation," *2019 Joint Conference of the IEEE International Frequency Control Symposium and European Frequency and Time Forum (EFTF/IFC)*, (2019), pp. 1–5.
37. S. Yanagimachi, K. Harasaka, R. Suzuki, M. Suzuki, and S. Goka, "Reducing frequency drift caused by light shift in coherent population trapping-based low-power atomic clocks," Appl. Phys. Lett. **116**(10), 104102 (2020).
38. A. Isakova, K. Savinov, N. Golovin, K. Sabakar, A. Dmitriev, and A. Rundau, "Combined Microwave and High-Frequency Modulation of the Injection Current of a Diode Laser for Mutiple-Frequency Excitation of CPT-Resonances," Russ. Phys. J. **63**(1), 171–175 (2020).
39. D. A. Paryohin, "Control Algorithms in Quantum Frequency Standards Based on the Effect of Coherent Population Trapping," Meas. Tech. **64**(1), 28–33 (2021).
40. M. I. Vaskovskaya, V. V. Vassiliev, S. A. Zibrov, V. P. Yakovlev, and V. L. Velichansky, "Spectral-Modulation Characteristics of Vertical-Cavity Surface-Emitting Lasers," Tech. Phys. Lett. **44**(1), 20–23 (2018).
41. M. I. Vaskovskaya, V. V. Vassilev, S. A. Zibrov, V. L. Velichansky, I. V. Akimova, A. P. Bogatov, and A. E. Drakin, "Amplitude/phase modulation and spectrum of the vertical-cavity surface-emitting laser output," Quantum Electron. **47**(9), 835–841 (2017).
42. G. Eisenstein and D. Bimberg, *Green Photonics and Electronics* (Springer, 2017).
43. K. Vahala and A. Yariv, "Semiclassical theory of noise in semiconductor lasers - Part I," IEEE J. Quantum Electron. **19**(6), 1096–1101 (1983).
44. K. Vahala and A. Yariv, "Semiclassical theory of noise in semiconductor lasers - Part II," IEEE J. Quantum Electron. **19**(6), 1102–1109 (1983).